7

PHENOMENOLOGY OF MAGNETOSPHERIC RADIO EMISSIONS

T. D. Carr, M. D. Desch, and J. K. Alexander

The radio spectrum of Jupiter spanning the frequency range from below 10 kHz to above 3 GHz is dominated by strong nonthermal radiation generated in the planet's inner magnetosphere and probably upper ionosphere. At frequencies above about 100 MHz, a continuous component of emission is generated by synchrotron radiation from trapped electrons between equatorial distances of about 1.3 and 3 R_J. This component exhibits a broad spectral peak at decimetric (DIM) wavelengths, distinct longitudinal asymmetries arising from asymmetries in Jupiter's magnetic field, and slow intensity variations that are presumably related to temporal changes in the energy, pitch angle, or spatial distributions of the radiating electrons. High resolution mapping of this component will probably continue to provide detailed information on the inner magnetosphere structure that is presently unobtainable by other means. Jupiter's most intense radio emissions occur in the frequency range between a few tenths of a MHz and 39.5 MHz. This decameter-wavelength (DAM) component is characterized by complex, highly organized structure in the frequency-time domain and by a strong dependence on the longitude of the observer and in some cases, of Io. The DAM component is thought to be generated near the electron cyclotron frequency in and above the ionosphere on magnetic field lines that thread the Io plasma torus, but neither the specific location(s) of the radio source(s) nor the specific plasma emission process are firmly established. At frequencies below about 1 MHz there exist two independent components of emission that have spectral peaks at kilometer (KOM) wavelengths. One is bursty, relatively broadbanded (typically covering 10 to 1000 kHz), and strongly modulated by planetary rotation. The properties of this bKOM component are consistent with a source confined to high latitudes on the dayside hemisphere of Jupiter. The other kilometric component (nKOM) is narrow banded, relatively weak, and exhibits a spectral peak near 100 kHz. The nKOM also occurs periodically but at a repetition rate that is a few percent slower than that corresponding to the planetary rotation rate. This component is thought to originate at a frequency near the electron plasma frequency in the outer part of the Io plasma torus (8 to 10 R_J) and to reflect the small departures from perfect corotation experienced by plasma there.

7.1. Introduction

The accidental discovery of the low-frequency Jovian radio emission by Burke and Franklin [1955] holds a special place in the history of solar system exploration. This discovery antedated many of the established historical landmarks, including the discovery of the Earth's radiation belts [Van Allen et al., 1958], the verification of the existence of a solar wind [Neugebauer and Snyder, 1962], and even the dawn of the space age itself in 1957. It foreshadowed a revolution in the thinking about the nature of planetary bodies and especially of their magneto-plasma environments. Considered at one time to be a 100 K gas giant surrounded by only the vacuum of space, Jupiter was soon realized to have a substantial magnetic field containing extensive energetic plasma capable of sustaining radio emission with brightness temperatures in excess of 10^{12} K. A discovery as fundamental as that of Burke and Franklin, but one which this time was not accidental, came in 1964 with the announcement by Bigg [1964] that some of the Jovian emission was directly influenced by the Galilean satellite Io. We now recognize Io as one of the solar system's most unusual members, but this

discovery was the first evidence that Jupiter and Io constitute a complicated electrodynamic system.

Jupiter has now been observed over 24 octaves of the radio spectrum, from about 0.01 MHz (10 kHz) to 300,000 MHz (300 GHz). Its radio emissions dramatically fill the entire spectral region where interplanetary electromagnetic propagation is possible at wavelengths longer than infrared. Three distinct types of radiation are responsible for this impressive radio spectrum. Thermal emission from the atmosphere accounts for virtually all the radiation at the high frequency end. Synchrotron emission from the trapped high-energy particle belt deep within the inner magnetosphere is the dominant spectral component from about 4000 to 40 MHz. The third class of radiation consists of several distinct components of sporadic low frequency emission below 40 MHz, much of which is presumably due to plasma instabilities in the inner magnetosphere that generate radiation slightly above the local electron cyclotron frequency. The nonthermal radiations led to the discovery of the magnetosphere over two decades ago, and they will remain for some time to come major sources of information regarding the magnetosphere and magnetic field of the planet. Although the thermal radio emission has yielded important information on the structure of the atmosphere underlying the magnetosphere [Berge and Gulkis, 1976], the interpretation of the thermal component lies outside the scope of this book.

In this chapter, our interest in the synchrotron and low-frequency components is twofold. First, they provide a means for probing the inner magnetospheric regions (inside $L = 3$) for which the only available in situ measurements are the very few given to us by Pioneer 11, with no prospect for additional ones for many years. Because the theory of the synchrotron emission process is well understood (unlike the low frequency emissions), the synchrotron component is an indispensable diagnostic tool for the study of the radiation belts within a few Jovian radii of the planetary body. Our second interest lies in the elucidation of the largely unexplained intricate phenomenology of the low frequency emission, in the hope of stimulating progress toward its eventual explanation in terms of one or more types of plasma instabilities. When that is accomplished, and the essential related details of emission and propagation are worked out, the low-frequency radiation too will become a useful diagnostic tool for the investigation of the inner Jovian magnetosphere.

Important historical milestones in the radio astronomical investigation of Jupiter are listed in Table 7.1, and a summary plot of the average power spectrum of its nonthermal emissions over the entire radio frequency range, with explanatory labeling, is presented in Figure 7.1. Some salient properties of the various Jovian nonthermal radio components are summarized in Table 7.2. The nomenclature and coverage of the standard radio engineering bands in which the emissions have been found are included in Figure 7.1. Each new component has been named for the band in which it was discovered, but none of the emissions are confined to a single band. There are two distinct subcomponents of the kilometric radiation, as will be explained in Section 7.4. Although the kilometric radiation is most likely distinct from the hectometric, it is not yet clear whether the latter should be considered a separate component from the decametric or merely an extension of it.

7.2. The decimeter wavelength emission

Early evidence for a Jovian magnetosphere: discovery of the synchrotron emission

The high degree of circular polarization of Jupiter's sporadic decametric bursts [Franklin and Burke, 1956] was the first indication of the Jovian magnetic field, although the significance of this early evidence was not widely recognized at the time.

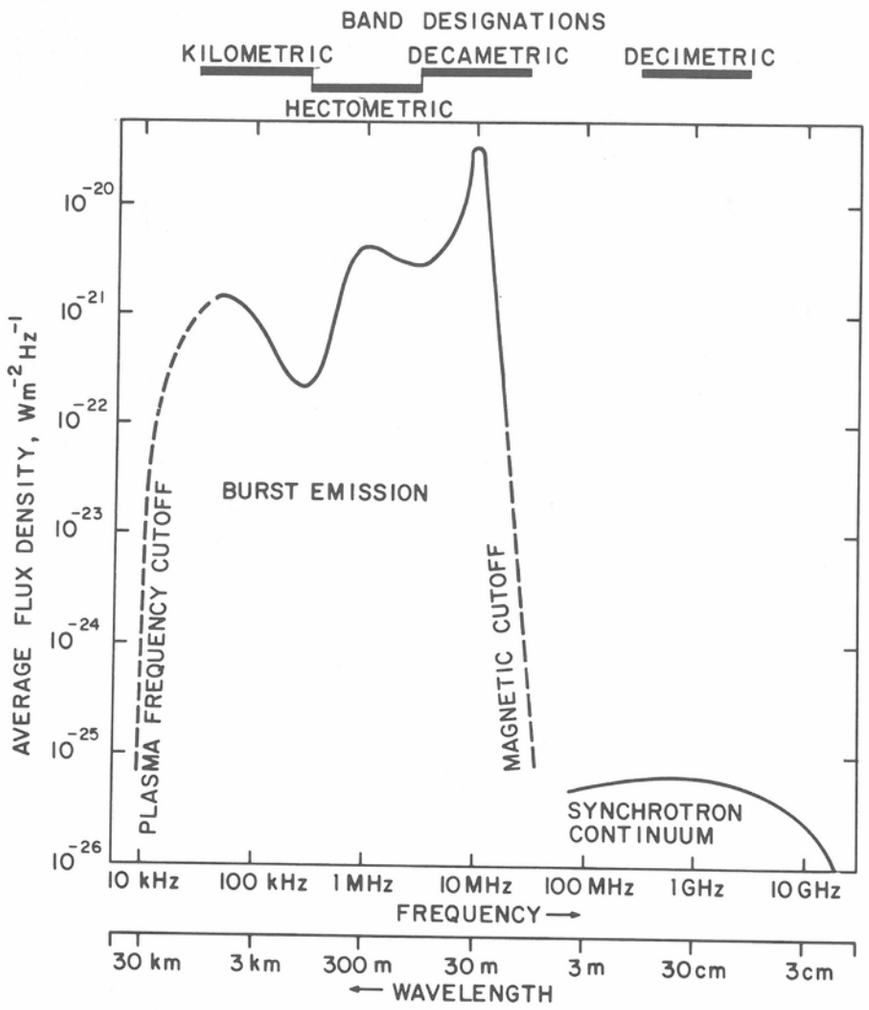

Fig. 7.1. The average power flux density spectrum of Jupiter's non-thermal magnetospheric radio emissions. Burst-component flux densities were averaged over inactive as well as active periods; the instantaneous spectrum may appear considerably different. The highest burst peaks attained values one to two orders of magnitude above the curve. The solid-line part of the burst-component curve is from Schauble and Carr (unpublished). The synchrotron-component curve is the difference between the total and thermal curves in Figure 7.2. Flux densities are normalized to a distance of 4.04 A.U.

For electromagnetic radiation to be polarized, the motions of the emitting particles must be subject to a systematic constraint. It is difficult to conceive of any such constraint acting on the source of naturally occurring radio emissions other than that exerted by an ambient magnetic field. The discovery of the Jovian nonthermal decimetric component [Sloanaker, 1959; McClain and Sloanaker, 1959] and the subsequent revelation by a number of observers of its more conspicuous properties, however, left no room for doubt of the existence of a planetary field. The properties are:

1. Continuous radiation rather than the sporadic bursts characteristic of the decametric component.

Table 7.1. *Historical milestones in Jupiter radio astronomy*

1950 – Decametric radiation (DAM) recorded by Shain at 18.3 MHz but not initially recognized.

1955 – DAM discovered by Burke and Franklin at 22.2 MHz.

1955–58 – first theories for the origin of DAM, including:
- electrostatic discharge noise from lightning in Jovian thunderstorms,
- ionospheric plasma waves generated by atmospheric turbulence, and
- ionospheric oscillations generated by volcanic shock waves.

1958 – nonthermal decimetric radiation (DIM) detected at wavelengths of 10 cm and longer.
– trapped energetic particles (Van Allen belts) detected in the terrestrial magnetosphere by Explorer-1 & 3 satellites.

1959–61 – DIM attributed to synchrotron radiation from energetic particles trapped in the tilted dipole field of the Jovian magnetosphere.
– DAM attributed to cyclotron radiation or cerenkov radiation by energetic electrons in the Jovian ionosphere.

1964 – Io influence on DAM discovered by Bigg.

1965 – first high resolution map of DIM obtained by Berge.
– terrestrial kilometric radiation (TKR) detected by USSR Elektron-2 satellite.

1963–69 – first applications of plasma kinetic theory to explanation of DAM.

1973–74 – first detection of Jupiter below 1 MHz with RAE-1 and IMP-6 satellites.
– first detailed studies of TKR with IMP-6 satellite.

1978–79 – full spectrum of Jupiter's low frequency emissions measured by Voyager.

2. A nonthermal spectrum that is nearly flat in the decimeter-wavelength band, but extends well into the microwave region where it overlaps the thermal component.
3. A distributed emission region that is centered on the planet and is roughly three Jovian diameters wide east-west and one diameter high north-south.
4. A linearly polarized component, amounting to 20 to 25% of the total intensity, most of the remainder being unpolarized.
5. A weak circularly polarized component that alternates between right- and left-hand polarization as the planet rotates.
6. An almost sinusoidal rocking of the plane of linear polarization of about $\pm 10°$ as the planet rotates, with the average orientation of the polarization plane perpendicular to the rotation axis.
7. A periodic variation in the total flux density as the planet rotates, generally with two maxima and two minima per rotation.

These clues clearly pointed to synchrotron emission by high energy electrons trapped in a Jovian Van Allen Belt [Drake and Hvatum, 1959; Roberts and Stanley, 1959; Field, 1959; Radhakrishnan and Roberts, 1960; Morris and Berge, 1962; Gary,

Table 7.2. *Components of Jupiter's radio spectrum*

Emission component	Decimetric (DIM)	Decametric–hectometric (DAM–HOM)	Broadband kilometric (bKOM)	Narrowband kilometric (nKOM)
Frequency range	< 80 MHz–300 GHz	~0.2–39.5 MHz	~10–1000 kHz	40–200 kHz
Polarization	~25% linear from 600 MHz to 5 GHz; ~1% circular at 1.4 GHz	Circular or elliptical; primarily RH above 20 MHz but mixed at lower frequencies	Circular or elliptical; emission centered near 200° CML is LH from above dayside and RH from over nightside	LH for northern magnetic latitudes, RH for southern magnetic latitudes
Peak flux density (4 A.U. equiv.)	$\sim 6 \times 10^{-26}$ W/m^2 Hz at 800 MHz	3×10^{-19} W/m^2 Hz at 10 MHz	$\sim 10^{-20}$ W/m^2 Hz at 60 kHZ	10^{-20} W/m^2 Hz at 100 kHz
Ave. isotropic equiv. total power	2×10^9 W	4×10^{11} W	$\sim 5 \times 10^8$ W	$\sim 10^8$ W
Dynamic spectrum	Smooth, continuous	Arc-shaped drifting features with duration of few min. at each frequency; occasional ms bursts at certain γ_1-CML	Short impulsive bursts superposed on slower drifts; longer duration at lower frequencies	Smooth, narrow-band emission repeatable at 3–5% slower than System III period
Origin	Synchrotron radiation from trapped electrons between 1.6 and 3 R_J	Plasma instability in auroral ionosphere and inner magnetosphere. Possibly R-X mode from Io plasma torus L-shells	Plasma instability in auroral ionosphere or inner magnetosphere. Possibly constrained to daytime sector with L–O mode	Plasma instability at low latitudes in inner magnetosphere near outer edge of Io plasma torus

Radiation by high-energy electrons in a magnetic field

A detailed treatment of synchrotron radiation theory as it is applied to astrophysics, with an extensive annotated reference list, is given by Pacholczyk, [1970]. Developments in the theory making it more readily applicable to the Jupiter problem have been made by Chang and Davis [1962], Korchak [1962], Thorne [1963], Ortwein, Chang, and Davis [1966], Legg and Westfold [1968], Clark [1970], Gleeson, Legg, and Westfold [1970], Degioanni [1974], and others. A qualitative understanding of most of the observed Jovian synchrotron emission phenomena, however, requires only a knowledge of the radiation characteristics of a single high energy electron in a magnetic field, a brief discussion of which is presented in this section.

If an isolated electron (of charge $-e$ and mass m_e) in a uniform magnetic field (**B**) is given an initial velocity (v) perpendicular to the field, where v is sufficiently small that the relativistic increase in mass with velocity is negligible, the electron will revolve in an almost circular path at $Be/(2\pi m_e)$ revolutions per second, in the sense of rotation of a right-hand screw advancing in the direction of **B**. Its orbit will not be precisely circular because of a relatively slow decrease in the radius of curvature due to the loss of energy (and velocity) by radiation. The frequency of revolution, however, will remain very nearly constant as the velocity and radius of curvature both decrease toward zero. Nearly monochromatic radiation will be emitted at the same frequency at which the electron is revolving. This frequency is the electron cyclotron frequency (or gyrofrequency), and is given by

$$f_c = \frac{Be}{2\pi m_e} \approx 2.8 \text{ B(Gauss) MHz} = 2.8 \times 10^4 \text{ B (Telsa) MHz} \qquad (7.1)$$

The radiation will be emitted in all directions, but its polarization will depend on the direction. Radiation propagating in the same direction as **B** will be right-hand (RH) circularly polarized, and in the opposite direction left-hand (LH) circularly polarized.* For all propagation directions within the plane of the orbit of the electron the polarization will be linear, with the polarization plane perpendicular to **B**. In other directions of propagation, the polarization will be RH or LH elliptical.

If the electron velocity is close enough to c that the mass increase due to relativity is appreciable, a relativistic beaming of the emitted radiation in the instantaneous direction of the velocity vector will also occur [Jackson, 1975]. This beaming is narrower the higher the electron energy, most of the power being radiated within an angle of $(1 - v^2/c^2)^{1/2}$ radians with respect to v. The half-power width of the instantaneous emission beam is given approximately by

$$\theta \approx 56/E \qquad (7.2)$$

* We use the right-hand screw rule for defining the RH polarization sense: The electric vector at each point in a fixed plane perpendicular to the propagation direction rotates in the same sense as a RH screw advancing in the direction of propagation. That is, rotation is counterclockwise when propagation is toward and viewed by the observer. For LH polarization, the electric vector of course rotates in the opposite sense. This is the convention that is generally used in radio astronomy and plasma physics, but is opposite to the one that until recently was used in physical optics.

where θ is in degrees and E is the electron energy in MeV. A distant observer in the plane of the electron orbit would see one pulse each revolution, as the beam swept past (if such an observation were possible). The emission beam pattern averaged over a full revolution (or many revolutions) would have a maximum in the orbital plane but would be constant in azimuth. The angular thickness of this radiation sheet would depend on the electron energy. For example, for a 20 MeV electron the half-power beam thickness of the sheet is about 2.8°, according to (7.2).

The instantaneous intensity seen by a distant observer in the orbital plane as a function of time can be represented by a Fourier series in terms of consecutive-integer harmonics of f_c (calculated from the relativistic mass of the electron rather than its rest mass). The power spectrum of the radiation from this single electon consists of a large number of narrow spikes separated by f_c. The envelope of these harmonics has a broad maximum at a frequency that is proportional to BE^2. As in the case of a low energy radiating electron, the polarization is linear when the electron orbit is seen edge-on, that is, when the line of sight is perpendicular to **B**. If the line of sight is along **B** (i.e., a face-on orbit) the radiation intensity is at a minimum because of the beaming effect, but whatever radiation is observed is RH circularly polarized if **B** points toward the observer. It is LH if **B** points away from the observer. For propagation in any other direction, the radiation is elliptically polarized; it contains both linearly and circularly polarized components (but no unpolarized component).

If the velocity of the electron is not perpendicular to **B**, its path is helical. The longitudinal and transverse components of **v** are $v \cos \alpha$ and $v \sin \alpha$, respectively, where α is the pitch angle. In this case, the direction of maximum radiation intensity is along the surface of a cone of opening angle 2α, and the synchrotron emission consists of integral harmonics of $f_c/\sin^2 \alpha$ rather than of f_c. The latter fact was not recognized until 1967 (see e.g., Scheuer [1968]), and as a result, a number of theoretical treatments of synchrotron emission published earlier are in error in some respects [Pacholczyk, 1970]. An observer in the path of the beam from a relativistic electron that is traveling along a helix with pitch angle α sees a broad spectrum (the envelope of the harmonics) with a maximum at approximately

$$f_{max} \approx 4.8\, E^2 B \sin \alpha \tag{7.3}$$

where f_{max}, E, and B are in MHz, MeV, and gauss (G), respectively. Thus, a 20 MeV electron with a 90° pitch angle in a magnetic field of 0.5 G emits a spectrum having a maximum close to 1000 MHz. The total power radiated by the electron, in watts, is approximately

$$p \approx 6 \times 10^{-22} E^2 B^2 \sin^2 \alpha \tag{7.4}$$

The observed synchrotron radiation comes, of course, from vast aggregates of electrons, rather than from a single one. The synchrotron-emitting electrons in a planetary magnetosphere with a primarily dipole magnetic field configuration are magnetically trapped, and there may be wide distributions of electron energy and equatorial pitch angle and magnetic field intensity and direction. All traces of the harmonic spike structure characteristic of the single-electron spectrum are of course smoothed out.

First-order explanation of the synchrotron emission phenomena

A "first order" explanation of the synchrotron emission phenomena, accounting for the early-observed effects listed previously, is given in this section. The explanation is based on the changing viewing geometry for trapped relativistic electron orbits in the

Jovian magnetic field as the planet rotates, assuming somewhat simpified orbits and field configuration.

The simplest useful approximation of Jupiter's magnteic field is that of a magnetic dipole located at the center of the planet, its axis tipped about 10° with respect to the planetary spin axis. The magnetic equator is thus tilted about 10° with respect to the spin equator. The belt of trapped charged particles is approximated by a shell about 2 R_J above the cloud-top level and centered on the magnetic equator. The synchrotron-emitting electrons follow paths that are relatively flat helices, that is, their equatorial pitch angles are not far from 90°. The mirror points of most of the electrons, at which the instantaneous pitch angles reach exactly 90°, are within about 1 R_J above and below the magnetic equatorial plane. The observed synchrotron emitting region is thus the projection upon the plane of the sky* of a toroidal source surrounding the planet. The width and height of the region are roughly 6 and 2 R_J, respectively. The long axis of the emitting region actually rocks $\pm 10°$ with respect to the rotational equator as the planet rotates, but this effect was not observed until considerably later when aperture-synthesis arrays of relatively high angular resolution became available [Branson, 1968].

The radiation seen along any line of sight is predominantly randomly polarized, with some residual linear component. When the line of sight to an element of volume in the emitting region is perpendicular to **B** at the volume element, the radiation from it will be linearly polarized in a plane that is perpendicular to **B**. However, **B** is not uniform. For the majority of the volume elements, the line of sight is not perpendicular to **B**, and the polarization will be elliptical. The polarization ellipse can have either sense and any of a wide range of axial ratios and major axis orientations. The superposition of the contributions from all the volume elements thus leads to predominantly unpolarized radiation with a residual linearly polarized component. (There is also a very small residual circular component, provided the resultant of the intensity contributions in one sense of elliptical polarization is greater than that of the other.) The polarization plane of the linear component is parallel to the plane of the magnetic equator. For qualitative visualization, it is convenient to think of the polarized component as having been radiated by electrons in circular orbits lying within the plane of the magnetic equator.

As the planet rotates, the intersection of the plane of the magnetic equator with the plane of the sky rocks back and forth by $\pm 10°$ relative to the spin equator, which remains fixed. This accounts for the observed $\pm 10°$ rocking of the plane of the linearly polarized component. The much weaker circularly polarized component was not investigated extensively until after these first-order effects were; it will be discussed later.

The observed variation in total flux density as the planet rotates is a manifestation of the beaming of the emitted radiation. For the simple dipole field model the beaming is maximum within the plane of the magnetic equator. When the *Jovicentric declination of the earth* D_E is zero, the earth lies in the plane of Jupiter's spin equator, and the magnetic equator would be seen on edge every 180° of rotation. (D_E is the angular distance of the earth from Jupiter's spin equator.) This would give rise to two flux density maxima of equal magnitude and spacing as the planet rotates. On the other hand, when D_E is positive (its possible values over Jupiter's 11.9 year orbital period range between $+3.3°$ and $-3.3°$), the two flux density maxima are separated by rotation intervals alternately less than and greater than 180°. When D_E is negative, the phase of alterna-

* For an observed region such as Jupiter's magnetosphere, which subtends a relatively small solid angle from Earth, the *plane of the sky* is perpendicular to the radius vector from an observer to an arbitrary reference point within the region.

tion of the narrower and wider rotation intervals is reversed. To a first approximation, this is what is observed. However, there are important departures from the predictions of this simple model; these will be discussed later.

Finally, the shape of the power spectrum of the synchrotron emission in the decimeter wavelength range is a consequence of the combined effects of several factors. These are:

1. the distribution of radiated power by a single electron as a function of frequency, direction, electron energy, electron pitch angle, and **B**;
2. the distribution of electron energies;
3. their pitch angle distribution;
4. their spatial distribution.

The electron energy distribution is one of the dominant factors. The spectral shape can be approximated from the power spectra of individual electrons in circular orbits seen edge-on as a function of their energies, together with the energy distribution of the electrons.

Present status of Jovian synchrotron phenomenology

It is not surprising that the great increase in resolution, sensitivity, and versatility of radio telescopes within the past decade has resulted in a greatly increased knowledge of the synchrotron emission phenomenology. There has also been considerable progress in emission region modeling. In the light of these relatively recent developments, we present in this section a brief overview of the phenomenology of Jupiter's synchrotron radiation, with emphasis on progress that has been made since the comprehensive review by Berge and Gulkis [1976]. The relatively large number of papers referenced in this review deal mainly with the synchrotron flux density spectrum and its variability, the central meridian longitude and magnetic latitude dependence of flux density, studies of the linearly and circularly polarized components, decimetric rotation period measurements, and relatively high-resolution mapping of the emitting region. Despite the fact that the emission mechanism is well understood and much is known of the general properties of the source, the detailed picture is still far from complete. As in the case of most reviews of active fields of research, recent results do not uniformly fall into neat and consistent patterns. The filtering action of time is usually needed to reconcile and refine new results.

Flux density spectrum. Figure 7.2 shows a plot of the flux density spectrum of the synchrotron emission and its region of overlap with the thermal component. The points were obtained from the compilations by Dickel et al. [1970] and Berge and Gulkis [1976], with additions from Gerard [1976], Shawhan et al. [1977], Gardner and Whiteoak [1977], Neidhofer et al. [1977], Werner et al. [1978] and de Pater [1980a, 1981c]. Much of the scatter is due to real long-term intensity variations.

An accurate separation of the synchrotron and thermal components of the radiation in the spectral region between about 1000 and 15 000 MHz is difficult. An accurate model accounting for one or the other component is required before a separation can be effected [de Pater, 1980b]. In the absence of such a model, several more approximate methods have been used [Berge and Gulkis, 1976]. In one such method, utilizing radio telescopes that are incapable of resolving the source region, the separation has been made on the basis of the polarization properties of the components [Roberts and Komesaroff, 1965; Dickel, 1967; Morris et al., 1968; de Pater, 1981c]. The thermal

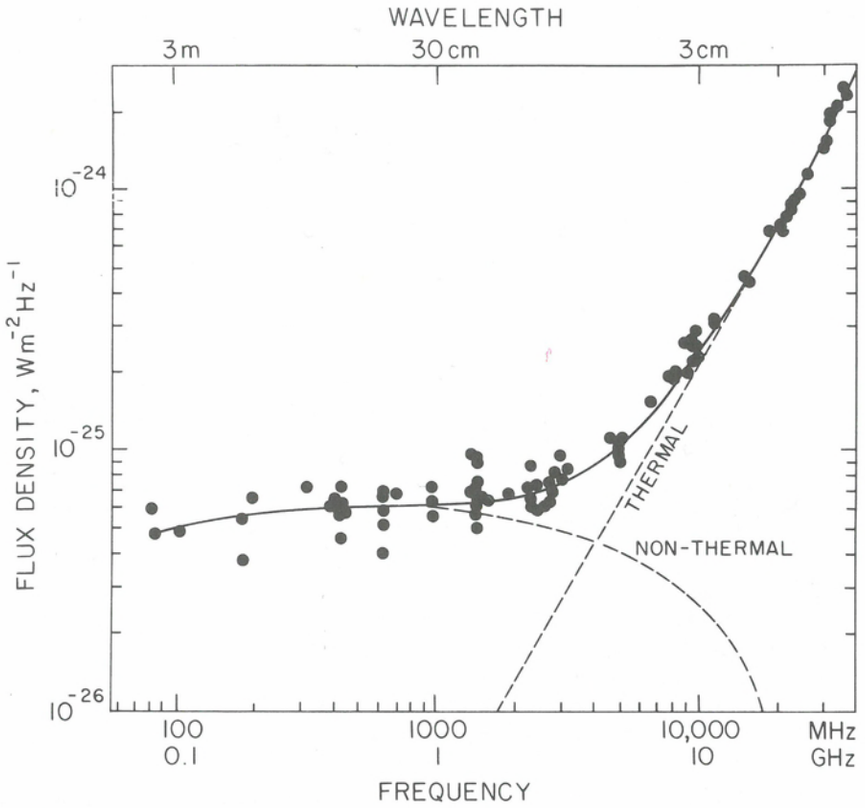

Fig. 7.2. Measurements of Jupiter's average flux density above 80 MHz. The dashed-line portion of the thermal component curve was made to fit points from de Pater [1980a, 1981c] corresponding to 320 K at 1410 MHz and 220 K at 4900 MHz, and to merge with the total flux density curve at higher frequencies. The dashed-line portion of the nonthermal curve was obtained by subtracting the thermal curve from the total curve. See text for references from which indicated points were taken.

component is assumed to be completely unpolarized; the overlapping nonthermal component is assumed to have the same degree of linear polarization that it has at lower frequencies where the thermal component is negligible. Then the flux densities of the two components separately can be calculated from the measured flux density and degree of linear polarization of the two combined. The deficiency in this method lies in the fact that the constancy of the degree of linear polarization of the nonthermal component becomes progressively more uncertain for frequencies above about 2000 MHz.

In other separation methods, employed with radio telescopes that at least partially resolve the sources, an approximate model is developed for (1) the entire synchrotron emitting region, (2) the part of the synchrotron emitting region in front of the visible disc, or (3) the thermal disc source alone. The approximate fractions of the total flux density due to the synchrotron and thermal components can then be ascertained [Berge, 1966; Branson, 1968; Beard and Luthey, 1973; Degioanni and Dickel, 1974; de Pater, 1980b].

The smooth curve in Figure 7.2 is an approximate fit to the points representing total flux density. The dashed curves approximate the separate flux densities of the two

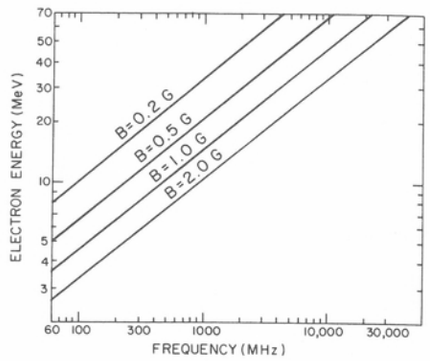

Fig. 7.3. Frequency of maximum synchrotron emission power for 90° pitch angle electrons as a function of electron energy and source magnetic field.

components in the region of overlap. The dashed thermal component curve was made to pass through points corresponding to disc temperatures of 320 K at 1410 MHz [de Pater, 1980a] and 200 K at 4900 MHz [de Pater, 1981c], and to merge with the total flux density curve at still higher frequencies. This dashed curve was then subtracted from the total intensity curve to obtain the dashed portion of the nonthermal curve in Figure 7.2, and also the corresponding portion of the curve in Figure 7.1. The unexplained long-term variations that are observed in the total flux density occur in the nonthermal component; the thermal component is presumably of much more nearly constant intensity (in time but not in frequency).

Our separation of the two components in Figure 7.2 depends critically on de Pater's estimates of the disc temperatures at 1410 and 4900 MHz. De Pater obtained the 1410 MHz temperature by developing a synchrotron source model based on her high-resolution maps (to be discussed later), and subtracting its contribution from the total observed flux density. She obtained the 4900 MHz temperature by assuming that the degree of linear polarization of the nonthermal component at 4900 MHz is the same as it is at 1410 MHz, at which frequency the thermal component is negligible, and then deducing the amounts of thermal and nonthermal radiation at 4900 MHz from the measured degree of linear polarization and flux density of the two combined.

In Figure 7.3 we have plotted the energy of a synchrotron-emitting electron with 90° pitch angle as a function of the frequency at which its radiated power is maximum, using (7.3), for each of a series of magnetic field values. Fields within this range are encountered in the actual emission belt, as mapped between about 1400 and 5000 MHz [e.g., Berge, 1966; de Pater, 1981] and assuming a dipole field with a magnetic moment of 4 GR_J^3 (4×10^{-4} T R_J^3) [Acuña and Ness, 1976c]. Thus in the 1 G region, most of the 1000 MHz radiation is emitted by approximately 14 MeV electrons, while that at 3000 MHz comes from electrons in the vicinity of 24 MeV.

The lowest-frequency measurements of the synchrotron radiation are those by Gower [1968] at 81.5 MHz and by Slee and Dulk [1972] at 80.0 MHz. The flux density in this region is only slightly less than at higher frequencies. Here most of the radiation comes from electrons of lower energies. Because mapping has not yet been possible at the lower frequencies, the magnetic field range in the 80 MHz emission region is not known. However, if 1 G can still be considered a typical value, then the majority of the electrons must have about 4 MeV energy. More likely, the field in most of the 80 MHz emitting region is somewhat less than 1 G, in which case the predominant electron energies are somewhat higher than 4 MeV. Although it has not been detected there, the synchrotron emission spectrum probably extends below 40 MHz, into the realm of the decametric bursts.

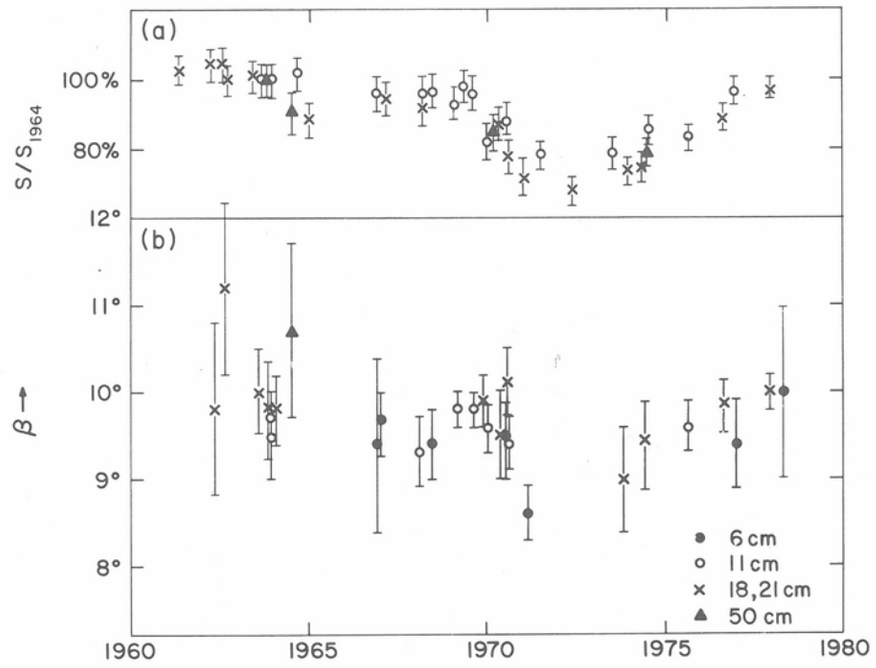

Fig. 7.4. (*a*) Variation of the total peak flux density S with time compared to the value measured in 1964.0. (*b*) Variation of β (as determined by de Pater's model-independent method) with time. Both compilations were made by de Pater [1981c].

Intensity fluctuations. During the first few years after the discovery of the Jovian synchrotron emission, relatively large and erratic intensity fluctuations on timescales of days or weeks were believed to be characteristic of the radiation. It was later concluded that they were not real but must have been due to background confusion effects or instrumental instabilities. However, in subsequent years occasional reports of longer period fluctuations continued to appear [e.g., Gerard, 1970; Klein et al., 1972]. Although there was at first some reluctance to return to the idea of variability, there is now no doubt of the existence of relatively large fluctuations in flux density on a timescale of years [Gulkis et al., 1973; Gerard, 1976; Berge, 1974; Klein, 1976; Hide and Stannard, 1976; Shawhan et al., 1977; de Pater, 1981c].

Figure 7.4*a* shows for several frequencies the variability of the ratio of the total flux density to that occurring at 1964.0 over a 17-year interval (after Hide and Stannard [1976] as updated by de Pater [1981c]). The data have been corrected for differences in distance and for systematic intensity variations with respect to central meridian longitude and magnetic latitude. The flux density decreased by 30% in a decade, clearly going through a minimum in 1972–1973. It is the synchrotron rather than the thermal component that has varied, for otherwise the brightness temperature of the thermal component would have had to change by an enormous amount. Klein [1976] states that there was no apparent correlation with solar activity. Moreover, the variations do not appear to be related to changes in D_E. According to Shawhan et al. [1977] the flux density varies in such a way that the shape of the spectrum changes. For example, their measurements reveal a pronounced spectral dip of about 15% near 1400 MHz which was not previously present. The data in Figure 7.4*a* do not bear this out, however,

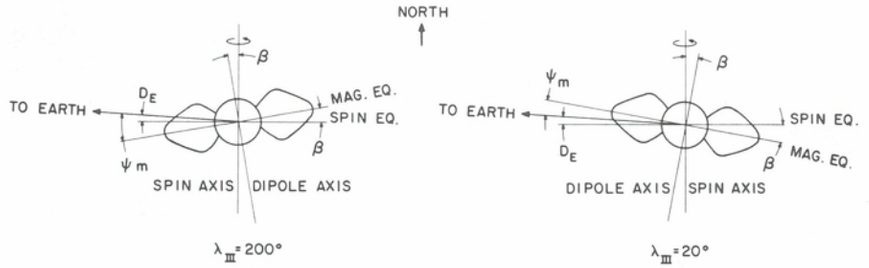

Fig. 7.5. Geometrical relationship between the dipole tilt angle β, the jovicentric declination of Earth D_E, and the magnetic latitude of the observer ψ_m, for the extreme cases when the observer's central meridian longitude λ_{III} is 200° and 20°.

perhaps because the points for the different frequencies in this figure are too sparsely distributed to show the effect.

In addition to the very slow intensity fluctuations that have been discussed, Gerard [1970] reported relatively rapid fluctuations occurring on time scales of days or weeks. During a 3 1/2-month period of intensive monitoring at 1408 MHz in 1974, Gerard [1976] observed two surges in intensity reaching a level 9% higher than the background, each with a half-intensity duration of about a week. Two or three smaller surges were also noted. He points out that the radial diffusion models of the magnetosphere cannot account for such rapid fluctuations, because the time constant for changes in the inner, stably trapped electron zone is predicted from the theory to be a few years [Coroniti, 1975]. Instead, he attributed them to some transient magnetospheric phenomenon such as substorms acting in addition to radial diffusion. Hill, Dessler, and Maher [1981] believe that significant changes in corotating convection patterns can occur over time intervals as short as 30 hr (see Chap. 10). Such changes would probably affect the synchrotron-emitting electrons and might therefore be related to Gerard's rapid fluctuations.

Whether or not Gerard's short-term fluctuations can be established as fact, the oberved long-term ones are undoubtedly manifestations of changes in the energy, pitch angle, or spatial distributions of the radiating electrons. Despite the fact that the deepest minimum in the curve in Figure 7.4*a* occurs within a year of the minimum in the 11.9 yr D_E cycle, the two curves are dissimilar elsewhere and are very likely unrelated. De Pater [1981c] has found some evidence in support of an earlier suggestion by E. T. Olson [de Pater and Dames, 1979] that the observed flux density decrease was due to a contraction of the radiation belts, or at least that the two effects were related. The discovery of the temporal spectral variations are of especial importance because of their potential utility as a means for monitoring one or more parameters of the radiation belt electrons. The fact that there is no apparent correlation with solar activity (see, however, the discussion in Sec. 7.3 of reported solar influence on low-frequency burst emission) should not be discouraging, because loading of the radiation belts is probably only very weakly dependent on the solar wind. Further observations of variability will be awaited with keen interest, and we anticipate increased theoretical activity stimulated by the need for a detailed explanation of the temporal effects.

The variation of flux density with central meridian longitude and magnetic latitude. Several of the parameters of the synchrotron radiation vary systematically as the planet rotates and are also influenced by the much slower periodic variation of the Jovicentric declination of the earth, D_E. As explained in Section 7.3, these effects are attributable to a predominantly dipolar configuration of the magnetic field in the radiation zone, the dipole axis being tipped about 10° with respect to the rotation axis. The clearest evidence for the 10° tipping is derived from the measurements of the linearly polarized component and will be discussed later. These effects are most easily described in terms of the central meridian longitude (CML) of the planetary disc as seen by the observer at a given time, and the magnetic latitude of the observer (ψ_m). The longitude system currently in use for Jovian radio and magnetospheric phenomena is designated System III (1965) and is based on a sidereal rotation rate of 870.536°/day (rotation

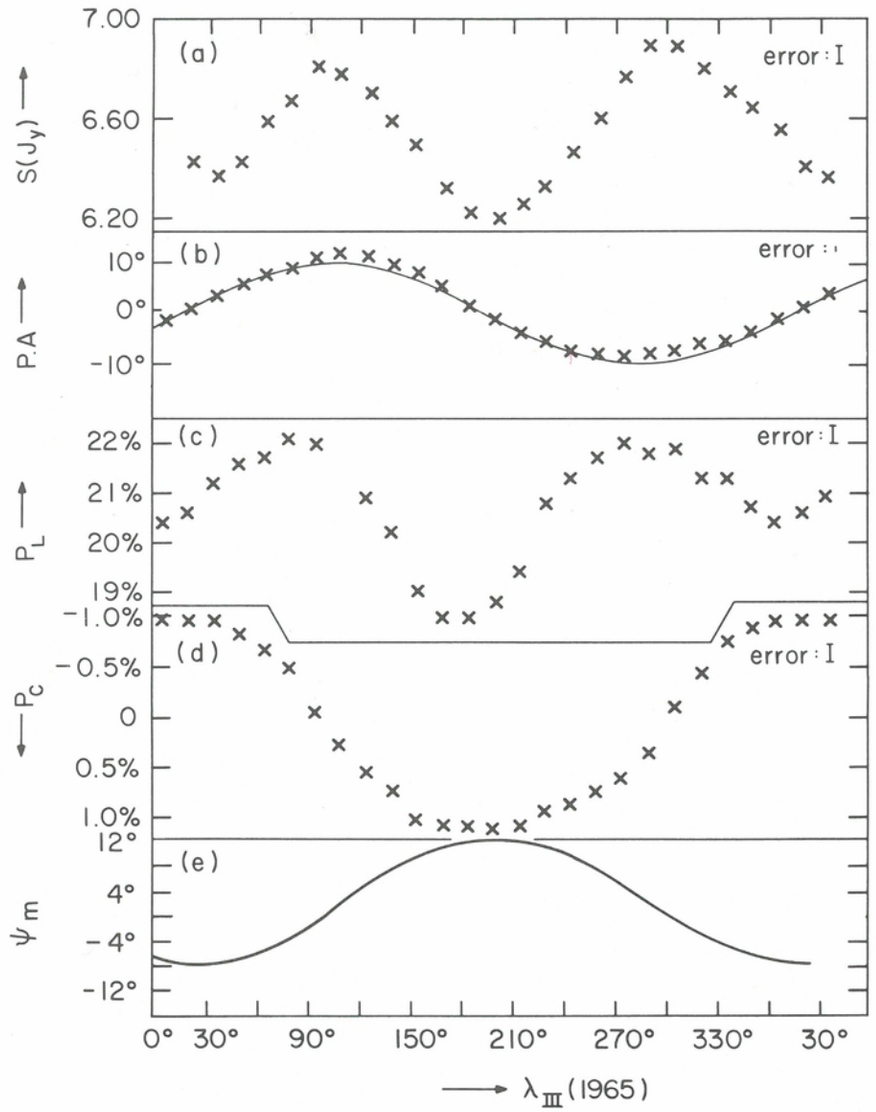

Fig. 7.6. Various parameters of the integrated radiation of Jupiter at 21 cm as functions of System III longitude. The north magnetic pole is assumed to be at 200°. (*a*) Total integrated flux density in Janskys, where 1 Jy = 10^{-26} W m^{-2} Hz^{-1}. (*b*) Position angle of the electric vector measured eastward from north in the sky. The smooth curve is defined by P.A. = 10° sin (λ_{III}-20°). (*c*) Degree of linear polarization. (*d*) Degree of circular polarization. (*e*) Magnetic latitude of Earth. Adapted from de Pater [1980a].

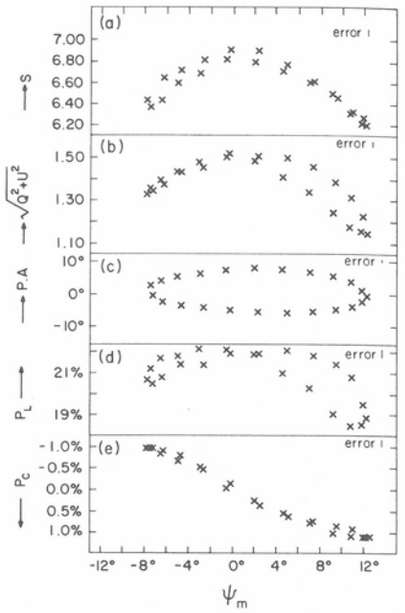

Fig. 7.7. The parameters of the integrated radiation of Jupiter as functions of the magnetic latitude of Earth with respect to Jupiter. (*a*) Total integrated flux density in Janskys. (*b*) Polarized flux density, $(Q^2 + U^2)^{1/2}$, in Janskys. (*c*) Position angle of the electric vector. (*d*) Degree of linear polarization. (*e*) Degree of circular polarization. After de Pater [1980a]. Positive P_c signifies the LH sense, and positive ψ_m indicates magnetic latitudes north of the magnetic equator. (In de Pater's original figures, the opposite sign convention for LH and RH is used.)

period ~9 hr 55 min 29.71 s). The value of the System III (1965) CML at a given time is designated by the symbol λ_{III}. (In addition to its use in specifying CML, the System III concept is extended to specify meridians that corotate with the planet and are not necessarily on the central meridian at the time under consideration.) The magnetic latitude of the observer is the angle between the magnetic equatorial plane, which is perpendicular to the assumed location of the dipole axis, and the radius vector from the center of the planet to the observer. For observations from Earth, the magnetic latitude of the observer is, to a good approximation,

$$\psi_m = D_E + \beta \cos (\lambda_{III} - \lambda_p) \tag{7.5}$$

where D_E is the Jovicentric declination of Earth (given in the *American Ephemeris and Nautical Almanac*), β is the assumed tilt of the dipole axis with respect to the axis of rotation, and λ_p is the value of λ_{III} toward which the northern-hemisphere pole of the magnetic dipole is tilted. Figure 7.5 illustrates the geometrical relationships between the quantities. Figure 7.6*e* shows a plot of ψ_m vs. λ_{III} as the planet rotates, for a time at which $D_E = 2.24°$. The values of λ_p and β for this plot are 200° and 10°, respectively. The choice of λ_p and β are model dependent, of course.

It appears that the measurements of integrated polarization parameters as a function of CLM that show the least statistical scatter are those of de Pater [1980a] obtained at 1412 MHz with the Westerbork Synthesis Radio Telescope in the Netherlands. The results of de Pater presented in Figures 7.6 and 7.7 will be used to illustrate the several longitude-correlated effects. Figure 7.6*a* shows the variation of total flux density with λ_{III}. This effect is most apparent at frequencies between about 1000 and 4000 MHz. It is caused by beaming of the emission [Morris and Berge, 1962; Gary, 1963] and has been extensively investigated by Roberts and Komesaroff [1965], Barber [1966], Roberts and Ekers [1968], Gulkis et al. [1973], Neidhofer et al. [1977] and de Pater [1980a, 1981c]. As mentioned previously, the radiation is assumed to a first approximation to be beamed in the plane of the magnetic equator, that is, at $\psi_m = 0°$. On the basis of the simple model, one would expect two maxima of equal heights in the

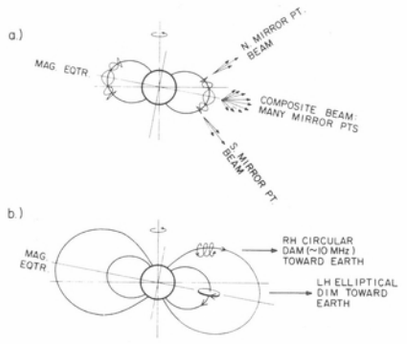

Fig. 7.8. (*a*) Beaming and (*b*) polarization geometry of emission by energetic trapped electrons gyrating in Jupiter's magnetic field.

curve of Figure 7.6a, with the peaks centered on the values of λ_{III} for which $\psi_m = 0°$, but with the two minima at different levels (except when $D_E = 0°$). It is apparent from (7.4) or Figure 7.6*e* that $\psi_m = 0°$ at $\lambda_{III} = 98°$ and 304°. Figure 7.6*a* indeed displays two peaks, centered at about $\lambda_{III} = 100°$ and 300°, in close agreement with the theory, but the peaks are of unequal shapes and heights. (It is only when $D_E = 0°$ that the two peaks are 180° apart.) It has been widely reported that the higher-longitude peak is the higher of the two. This is one of many second-order effects not accounted for by the simple tilted-dipole field model.

In Figure 7.7*a* the total flux density is plotted as a function of ψ_m instead of λ_{III}. For a dipole model in which none of the radiation is blocked by the planet, the points would like on a single arch-shaped curve that is symmetrical except it would extend farther for positive than for negative ψ_m values, because $D_E > 0°$ (see Fig. 7.5). If the electrons in such a model were monoenergetic, all with an energy of, say, 20 MeV, and if they had equatorial pitch angles of exactly 90°, the half-flux- density width of the flux density vs. ψ_m curve would be about 3°, as given by (7.3). The fact that the curve in Figure 7.7*a* is much wider than this is due to several factors, the principal ones of which are that there are distributions rather than single values of equatorial pitch angle (α_e) and electron energy. Those electrons with α_e considerably different from 90° make helical excursions to and from mirror points well above and below the magnetic equator. Most parts of the helical paths of these electrons are appreciably inclined with respect to the equatorial plane and therefore emit radiation that is not beamed closely to it. The width of the beam must be at least as great as the angle of intersection of the electron orbital planes at pairs of conjugate mirror points that are farthest above and below the magnetic equator (not considering shadowing by the planetary body). This effect is illustrated in Figure 7.8*a*. The presence of relatively low energy synchrotron-emitting electrons also tends to widen the beam, as does the presence of multipole field components.

The function indicated by the points in Figure 7.7*a* is actually double valued, neither branch of which is symmetrical about $\psi_m = 0$. Thus, the shapes of the parts of the beam above and below the magnetic equator are different, and the latitudinal profile of the beam changes somewhat with longitude. For the dipole model on which the plot in Figure 7.6*e* is based, the System III (1965) longitudes 200° and 20° define a plane of symmetry. The points in Figure 7.6*a* are not symmetrical about longitude 20° (where ψ_m is minimum), although they are more nearly so about 200° (where ψ_m is maximum); this is the same effect as the splitting into two arches seen in Figure 7.7*a*.

The difference in the beam profile for northern and southern magnetic latitudes has long been observed. This difference depends on D_E. When $D_E > 0°$, the decrease in S with increase in $|\psi_m|$ northward from the magnetic equator is more steep than it is

when $|\psi_m|$ increases southward from the equator. The reverse is true when $D_E < 0°$ [Roberts and Komesaroff, 1965; Gulkis et al., 1973]. Degioanni [1974] showed that this effect is probably caused by the asymmetrical blocking by the planet of much of the radiation from the back side of the emission region when $D_E \neq 0°$. Figure 7.5 will aid in visualizing it. The other asymmetries that are observed are attributed to the multipole field components, in combination with planetary shadowing, as discussed later in this section.

Polarization. Over the frequency range from 600 MHz or below to at least 5000 MHz, the nonthermal component is about 75%–80% unpolarized and about 20%–25% elliptically polarized. The shape of the polarization ellipse changes as the planet rotates, and its polarization sense reverses twice each rotation. (The polarization ellipse is the locus of the tip of the electric vector of the polarized component during each cycle as the wave passes.) The ellipse for this radiation is always thin, the ratio of its major to minor axis lengths (axial ratio) never being less than about 40. The minor axis momentarily becomes zero at each reversal of sense. The major axis remains very nearly perpendicular to the magnetic dipole axis during rotation (to within $\pm 1°$ or less).

Before proceeding with the discussion of the linearly polarized component, we shall dwell briefly on general methods for specifying polarization. A set of four parameters is required to specify the intensity and polarization state of partially polarized radio emission. Many equivalent sets are possible. The two sets which are used most often for Jupiter are as follows:

1. Total flux density (S), degree of linear polarization (P_L), degree of circular polarization (P_C) with sign to indicate sense, and position angle of the plane of linear polarization (P.A.).
2. The four Stokes parameters, I, Q, U, and V.

P_L and P_C are the fractions of the total flux density that are linearly and circularly polarized, respectively. They pertain to the linear and circular parts of the polarization ellipse. The Stokes parameter I is simply the total flux density, S. The polarized part of S is $(Q^2 + U^2 + V^2)^{1/2}$; the linearly and circularly polarized parts are $(Q^2 + U^2)^{1/2}$ and V, respectively. The sign of V specifies the polarization sense; $-$ is for right hand (RH) and $+$ is for left hand (LH). The tilt angle of the major axis of the polarization ellipse, with respect to the x axis, is $(1/2) \tan^{-1}(U/Q)$. (In the coordinate system that is assumed, propagation is in the $+z$ direction, and the x axis is in such a direction that $Q > 0$ and $U = 0$ for a wave that is linearly polarized in the xz plane.) The axial ratio of the ellipse is the cotangent of $(1/2) \sin^{-1}[V/(Q^2 + U^2 + V^2)^{1/2}]$. Typical values of P_L and P_C for Jupiter's nonthermal decimetric radiation are 0.25 and 0.01, respectively, so that $(Q^2 + U^2)^{1/2} = 0.25S$ and $V = 0.01S$, where S is the total flux density of only the nonthermal part. If the thermal component were included with the nonthermal, P_L and P_C would of course be smaller. Thus, the axial ratio of the polarization ellipse in this case is approximately cot $[0.5 \sin^{-1}(0.01/0.25)]$, or 50. The principal advantage in using Stokes parameters instead of a more easily visualized set of quantities results from their additive property: if several independent waves propagating in the same direction are superimposed, the Stokes parameters of the resultant wave are the sums of the corresponding Stokes parameters of the individual waves. This property greatly facilitates the matching of assumed models of a distributed source of partially polarized radiation, such as Jupiter's magnetosphere, to the observed integrated Stoke's parameters. For additional information on Stokes parameters see Kraus [1966] and references cited therein.

The linearly polarized component. Figure 7.7*b* shows the linearly polarized component of the flux density, which in terms of Stokes parameters is $(Q^2 + U^2)^{1/2}$, plotted as a function of the magnetic latitude ψ_m. The variation with ψ_m is significantly different from that for the total flux density in Figure 7.7*a*. A difference is to be expected because most of the linearly polarized radiation comes from the magnetic equatorial region and is relatively sharply beamed within the equatorial plane whereas the total flux density contains the radiation from outside the equatorial plane as well. The latter is the sum of elementary contributions having a wide range of emission beam directions and polarizations, and therefore the resultant beam is broadened and has a lower degree of linear polarization.

Measurements of the variation of the plane of linear polarization with CML have been made by Morris and Berge [1962], Gary [1963], Roberts and Komesaroff [1965], Komesaroff and McCulloch [1967], Morris et al. [1968], Roberts and Ekers [1968], Whiteoak et al. [1969], Berge [1974], McCulloch [1975], Stannard and Conway [1976], Gardner and Whiteoak [1977], Neidhofer et al. [1977, 1980], de Pater [1980a, 1981c], and Komesaroff et al. [1981]. Such meaurements provide the best means for determining the tilt β of the equivalent magnetic dipole, and they have the potential for yielding more detailed information on the structure of the field in the vicinity of the magnetic equator than do the other CML-related quantities. Figure 7.6*b* shows, for the 1412 MHz data of de Pater, the position angle (P.A.) of the plane of linear polarization relative to the plane of the rotational equator, plotted as a function of λ_{III}. It is clear from this figure that the polarization plane rocks back and forth by approximately $\pm 10°$ with respect to the rotational equator. Because the polarization plane is parallel to the magnetic equatorial plane in the simple dipole model, the value of the tilt angle β of the dipole axis with respect to the rotation axis must also be approximately 10° (see Fig. 7.5). The smooth curve in Figure 7.6*b* is the calculated position angle of the dipole model magnetic equatorial plane, relative to that of the spin equator, plotted as a function of λ_{III}. The departure of the measured points from the calculated curve is a clear indication of the limitations of the model. Figure 7.7*c* shows the variation of P.A. with respect to ψ_m. The quasielliptical curve defined by the points in this figure is approximately symmetrical about the vertical line $\psi_m = D_E = 2.24°$, but this symmetry and that about the horizontal line P.A. $= 0°$ are both imperfect.

Roberts and Komesaroff [1965] and most of the other authors referenced above have found it useful to evaluate the amplitudes and phases of the least squares Fourier series fit to the measured P.A. vs. λ_{III} curves. The series can be expressed in the form

$$\text{P.A.} = A_0 - A_1 \sin(\lambda_{III} - \ell_1) - A_2 \sin 2(\lambda_{III} - \ell_2) - A_3 \sin 3(\lambda_{III} - \ell_3) \qquad (7.6)$$

Here the amplitude A_1 can be identified with the tilt angle (β) of the dipole axis of the dipole-approximation field model, and the phase ℓ_1 with the System III longitude toward which the northern-hemisphere end of the dipole axis is tipped. Significant values of amplitudes and phases of at least the first two sinusoidal terms can generally be determined when the measurements are made under suitable circumstances. For example, for measurements made during October 1975 at 2700 MHz [Komesaroff and McCulloch, 1975] the amplitudes and phases of the first three and the fifth sinusoidal terms were as given in Table 7.3. Values for the other terms were not of sufficient statistical significance to be listed.

Gardner and Whiteoak [1977] and Neidhofer et al. [1980] report a slight change in the indicated value of A_1 as a function of frequency, the value ranging from about 10° at 1400 MHz to about 9° at 5000 MHz. This effect, Gardner and Whiteoak suggest, may indicate that the overall distribution of synchrotron radiation changes with frequency. This would be consistent, they point out, with theoretical predictions

Table 7.3. *Fourier amplitudes and phases of polarization position angle as a function of CML; measurements at about 2700 MHz during October 1975 [Komesaroff et al., 1980]. All quantities are in degrees.*

Amplitude	Std. error	Phase	Std. error
$A_1 = 9.85$	0.04	$\ell_1 = 195.3$	0.2
$A_2 = 1.16$	0.04	$\ell_2 = 174.9$	1.1
$A_3 = 0.19$	0.04	$\ell_3 = 202.0$	4.3
$A_5 = 0.16$	0.04	$\ell_5 = 177.7$	3.0

[e.g., Beck, 1972] that the most energetic electrons will be found to be more concentrated toward the planetary surface, and with the Pioneer in situ measurements, which seem to support the prediction [e.g., Fillius, 1976]. More recently, Komesaroff et al. [1981] also found an apparent decrease in A_1 with increasing frequency, but it was only half as large as that reported previously and was of marginal statistical significance.

De Pater [1980b] has reached a quite different conclusion regarding the variability of β. She found the emission regions at 1412 MHz and 4885 MHz to be of essentially the same size and shape, and concluded that the reported changes in β with frequency may be temporal changes instead. She recalculated β from all available previously published data on the basis of the maximum peak-to-trough excursion of the P.A. vs. λ_{III} curve, instead of using the customary least squares fit of the fundamental Fourier term to the data. The resulting curve of β vs. time over a 16-year interval, including de Pater's own data, is shown in Figure 7.4*b*. A comparison of the curves in Figures 7.4*a* and 7.4*b* strongly suggests a correlation of β with flux density. De Pater points out that the two brightest regions on synchrotron source maps were apparently closer together over a span of a few years that included the time of the observed flux density reduction than they were either before or after that interval [de Pater, 1980b]. She offers as a possibility the suggestion that the minima in the curves of both Figures 7.4*a* and 7.4*b* result from a contraction of the emission region. The fact that during the flux density minimum a larger proportion of the radiation seems to have come from closer to the planetary body, where the multipolar field effects are more pronounced, was perhaps the cause of the observed change in β. This is a most interesting idea. The accumulating evidence for the long-term aperiodic variability of the synchrotron emission parameters will no doubt stimulate new measurement programs.

Progress has also been made in accounting for the Fourier harmonics above the fundamental. The earliest efforts in this regard were those of Conway and Stannard [1972], Komesaroff and McCulloch [1975], Gerard [1976], and Gardner and Whiteoak [1977]. Gerard showed that when the shadowing of radiation from behind the planet is taken into consideration, the quadrupole field component can give rise to the second harmonic term. He suggested that the "charged particle equator" (i.e., the surface of minimum B within which particles having 90° equatorial pitch angle would lie) is warped rather than planar in a particular longitude sector. He succeeded in calculating the λ_{III} values at which the nulls in the second harmonic term occur from the magnetic quadrupole moment as measured in situ by Pioneer 11 [Acuña and Ness, 1976c].

Smith and Gulkis [1979] were able to derive a curve of P.A. vs. λ_{III} from the Pioneer 11 magnetic field measurements which was in good agreement with the measured curve. They assumed that only electrons lying in the non-planar equatorial surface (charged particle equator) at a distance of about 2 R_J from the center of the

planet need be considered, and that beaming is unimportant but that planetary shadowing must be accounted for. They concluded that the prospects for using radio data to improve the magnetic field model are promising.

Komesaroff and McCulloch [1981] showed that a good approximation to the amplitudes and phases of the first two sinusoidal terms of the Fourier series fit to the 16-year Komesaroff et al. [1981] data set could be derived from Pioneer 11 magnetic field measurements. The dipole and quadrupole field components were used, and planetary shadowing of emitted radiation was taken into account. There was good agreement in the case of the second harmonic amplitude only when it was assumed that the distance of the emitting shell of electrons was between 1.5 R_J and 2 R_J from the center of the planet. They concluded that the form of the position angle curve is relatively insensitive to any variation in the pitch angle distribution, but it depends sensitively on the magnetic field structure, at least on the dipole and quadrupole components in the region between 1 R_J and 2 R_J.

Birmingham [1981] followed the approach taken by Smith and Gulkis [1979], starting with basically the same assumptions, but his calculations were more detailed. For both the 0_4 magnetic field model and the P10-11 model derived from Pioneer 10 and 11 field measurements combined [Smith and Gulkis, 1979], he calculated the Fourier amplitudes and phases for each of a series of values of the effective distance of the radiating electrons (in the warped magnetic equatorial surface) from the center of the planet. Birmingham stated that although there was good qualitative agreement of his calculated results with the observations, there were several types of quantitative disagreements. It was apparently not possible to determine definitely which was the most realistic of the assumed distances of the equivalent ring of emitting electrons from the center of the planet, nor which of the two magnetic field models gave the better result. He concluded that although the model can be refined in several ways, further effort employing this particular approach is probably not justified at present because of the uncertainties in the radio, magnetic field, and energetic electron data used.

In summary, the dependence of linear polarization position angle on CML as modeled from the Pioneer 11 magnetic field measurements by Gerard, Smith, and Gulkis, Komesaroff and McCulloch, and Birmingham is in each case in good qualitative agreement with observation. However, only Birmingham's work appears sufficiently detailed to reveal the severe limitations on the use of this type of radio data for improving existing models of the magnetic field and the high energy particle distributions. Clearly, the high-resolution intensity and polarization parameter maps of the emission region would provide a sounder basis for model development than do the measurements of integrated polarization parameters utilized in the preceding papers. As we shall see, relatively high-resolution maps have recently been made and have indeed been used with apparent success in model development.

Figure 7.6*c* shows the variation of the *degree* of linear polarization P_L (ratio of linearly polarized flux density to total flux density) with respect to λ_{III}. The two maxima in P_L occur very nearly at the zero crossings of ψ_m, and hence they coincide with the maxima in the total flux density curve in Figure 7.6*a*. P_L has minima when Earth is farthest above and below the magnetic equatorial plane. If D_E had been zero the two minima, occurring at $\lambda_{III} = 190°$ and 360°, would probably have reached nearly equal levels. Figure 7.7*d* shows the corresponding variation with respect to ψ_m. As Berge and Gulkis [1976] have pointed out, the similarity of the curve of P_L vs. λ_{III} to that of total flux density vs. λ_{III} (Fig. 7.6*a*) indicates that the linearly polarized component is more sharply beamed than is the total emission. If the beaming of the two were the same, their intensities would vary proportionally, and the ratio P_L would remain constant

instead of varying as it actually does. The total radiation thus consists of (1) an unpolarized nonthermal component that is beamed, (2) a polarized nonthermal component that is more sharply beamed, and (3) a thermal component that is unpolarized, not beamed, and is relatively small at frequencies below 2000 MHz. No variation in the degree of linear polarization of the nonthermal component with respect to frequency has yet been found, although such a variation is probable in both the lowest and highest frequency regions of the observable synchrotron spectrum.

The circularly polarized component. High energy electrons in a tilted Jovian dipole field with equatorial pitch angles (α_e) near 90° direct most of their synchrotron radiation close to the plane of the magnetic equator. In these directions the polarization is linear, or at least elliptical with a high axial ratio. For propagation directions farther out of the equatorial plane, where the intensity is less, the axial ratio is also less, making the polarization ellipse more nearly circular. Thus, although the degree of linear polarization (P_L) is greatest for propagation directions parallel to the equatorial plane, the absolute value of the degree of circular polarization ($|P_C|$) is greatest in propagation directions which are most nearly perpendicular to it. Now if in addition there are other electrons having an extended range of α_e values both less and greater than 90°, major parts of their helical paths are more or less steeply inclined with respect to the magnetic equatorial plane, as suggested in Figure 7.8*a*, causing (1) a broadening of the curve of S vs. ψ_m, (2) a reduction in the amplitude of the curve of P_L vs. ψ_m, with an increase in the relative amount of unpolarized radiation, and (3) an increase in the amplitude of the curve of P_C vs. ψ_m. The reason for the latter is that the farther the mirror points of electrons near the central meridian are from the magnetic equator (and hence from the Earth direction), the more nearly perpendicular is the line of sight from Earth to the orbital planes of the mirroring electrons. Each electron emits most of its radiation from the vicinity of the mirror points, where it spends most of its time. The circularly polarized components of opposite sense from conjugate pairs of mirror points are of equal intensity when $\psi_m = 0$, so that their net contribution to the circular polarization is zero. However, when $|\psi_m|$ is maximum, one of the mirroring orbits is seen more nearly face-on than the other, and $|P_C|$ then reaches a maximum.

The sign of P_C is positive, corresponding to the LH sense, if **B** projected onto the line of sight is away from the observer; it is negative (RH) if the **B** component is toward the observer.

Measurements of the degree of circular polarization of Jupiter's synchrotron radiation have been made by Berge [1965, 1974], Seaquist [1969], Komesaroff et al. [1970], Stannard and Conway [1976], Roberts and Komesaroff [1976], Biraud et al. [1977], Neidhofer et al. [1977, 1980], and de Pater [1980a]. Figure 7.6*d*, from de Pater's 1412 MHz measurements, shows the degree of circular polarization, P_C, as a function of λ_{III}. The two zeros in the P_C curve occur at λ_{III} values of approximately 100° and 300°, about the same longitudes at which the maxima in the S (Fig. 7.6*a*) and the P_L curves (Fig. 7.6*c*) occur. It is apparent from Figure 7.7*e* that the zeros of P_C lie close to $\psi_m = 0°$, in agreement with the qualitative picture of the emission process presented above. The two absolute-value maxima of the P_C curve occur very nearly at the propagation directions which are farthest above and below the magnetic equatorial plane, nearly in coincidence with the S and P_L minima, again in close agreement with our qualitative picture.

The tendency for the curve of P_C vs. ψ_m (Fig. 7.7*e*) to become flattened, that is, more nearly horizontal, the farther ψ_m is from zero was first observed by Biraud et al. [1977] and Roberts and Komesaroff [1976], and has subsequently been observed by others.

Roberts and Komesaroff attribute this characteristic shape to the pitch angle distribution of the radiating electrons. Using a thin L-shell emission model, they were able to adjust the *shape* of the theoretically derived curve of P_C vs. ψ_m by altering the pitch angle distribution function, and to adjust the *amplitude* of the curve by manipulating the assumed value of the equatorial magnetic field **B** within the L-shell. The value they obtained is 0.3 G. This can be considered a first approximation to the mean value of **B** for the actual distributed emitting region weighted by the brightness. The high resolution mapping of de Pater and Dames [1979] indicated, however, that the synchrotron emission peak in the equatorial plane was at about 1.3 R_J, decreasing to half brightness at about 3.4 R_J. Thus, the actual emission region is far more extended and complex than the thin shell model upon which the radio determination of **B** was based. In order to obtain radio measurements of **B** at a particular point to within accuracies better than, say ±50%, a more realistic model of the emission region will have to be used.

In a discussion of the same radio observations, Roberts [1976] concluded that theoretically derived curves of S vs. ψ_m and P_L vs. ψ_m are much less sensitive to the nature of the pitch angle distribution than is the P_C vs. ψ_m curve. He also pointed out that only the latter curve provides a means for measuring **B**.

Still another important piece of information that can be deduced from measurements of P_C as a function of ψ_m is the sense of the magnetic dipole, that is, whether the majority of **B** field lines emerge from the northern or the southern Jovigraphic hemisphere. Berge [1965], who first measured the circularly polarized component, found that it emerges from the northern hemisphere, opposite to the direction of the terrestrial field relative to the rotational angular velocity vector of the planet. This same conclusion had previously been reached by Warwick [1963a] and Dowden [1963] on the basis of measurements of the decametric radiation, after having made certain unverified assumptions regarding the unknown decametric emission mechanism. In arriving at his conclusion, Berge found that the circularly polarized component is LH when Earth is north of the magnetic equator and RH when south of it. This is apparent in Figure 7.7*e*. When Earth is at its maximum northern magnetic latitude, for which λ_{III} is 201°, the northern-hemisphere magnetic pole is tipped toward the observer. As we have previously stated, most of the circularly polarized radiation comes from the vicinity of electron mirror points in the region near the central meridian. The polarization sense of the integrated wave contributions of all these electrons, which have a symmetrical distribution of α_e values centered on 90°, is the same as it would have been if they all remained in the magnetic equator, with α_e values of exactly 90°. Thus, we can use the circular orbit shown in the magnetic equator in Figure 7.8*b* to deduce the direction of **B**. The pertinent facts are (1) in an orbit seen obliquely from its northern face the electron emits LH elliptical radiation and (2) for radiation having the LH sense, the direction of **B** projected onto the line of sight must be away from the observer. It follows that field lines must penetrate the electron orbital plane from its northern side, as shown in Figure 7.8*b*, and therefore that the majority of **B** lines emerge from the northern Jovigraphic hemisphere of the planet and enter the southern hemisphere. This was essentially Berge's line of reasoning. As we discuss further in Section 7.3, an earlier analysis of the low-frequency burst emissions led to the same conclusion.

Decimetric rotation period measurements. The rotation period of Jupiter's inner magnetosphere can be determined from both the decametric burst emission (below 40 MHz) and the decimetric synchrotron emission. Such measurements by both methods have been made for a number of years. As techniques have improved, the decimetric

and decametric measurements have tended to converge, providing the basis for establishing the currently accepted value, designated System III (1965). This value is 9 hr 55 min 29.71 s [Riddle and Warwick, 1976]. Although the mean of the better decimetric measurements [Berge and Gulkis, 1976] appeared to be slightly different from the best at decametric wavelengths [Carr and Desch, 1976 and references therein], more recent results have essentially eliminated the discrepancy.

The method for arriving at the rotation period from synchrotron emission data involves the determination of fundamental periodicities in measurements of the linear-polarization-plane position angle as a function of time or in measurements of the degree of circular polarization as a function of time. The position angle method has been used much more extensively than that based on circular polarization. One way of calculating the period from decimetric position angle measurements is to vary (in small increments) the assumed period upon which λ_{III} in the Fourier series fit (7.6) is based, until the phase ℓ_1 of the fundamental term attains a maximum or minimum value. The best decimetric rotation period measurement is that of Komesaroff et al. [1981], based on over 16 years of linear polarization position angle measurements at three observatories. This value agrees with the System III (1965) value to within 0.02 s. Very nearly the same result has been obtained from measurement of the circularly polarized component. Biraud et al. [1977], using their own measurements of this component at 1400 MHz together with the earlier data of Komesaroff et al. [1970], Berge [1974], and Seaquist [1969], obtained the value 9 hr 55 min 29.69 s ± 0.12 s. This is not significantly different from the System III (1965) value nor from the above determined from position angle measurements.

The rotation period measured by Komesaroff et al. [1981] at decimetric wavelengths and that by May, Carr, and Desch [1979] at decameter wavelengths (see Sec. 7.3) both differ from the System III period by only 0.02 s. An error of 0.02 s in the value assumed would cause the apparent longitudes of features corotating with the inner magnetosphere to drift only 10° in 50 yr. Differential magnetic rotation between the synchrotron and decametric regions ($r < 4\ R_J$) must be very slight if it exists at all.

Source mapping. The first measurements yielding information on the spatial distribution of the Jovian decimetric source were the interferometric observations of Radhakrishnan and Roberts [1960] and Morris and Berge [1962]. Berge [1966], by fitting a model to data obtained with the Owens Valley Radio Observatory interferometer, produced a two-dimensional brightness distribution map of the synchrotron-emitting region which in its gross structure is remarkably similar to the best available today. Berge had assumed a highly symmetrical model, and as a result his map does not display irregularities attributable to nondipolar field components; a 10° tilt of the dipole was built into his model. Barber [1966] and McAdam [1966] also made interferometric measurements of the emission region. Branson [1968] used the method of aperture synthesis to produce three two-dimensional maps at equally spaced intervals of CML. His maps clearly show the wobble of the magnetic equator with rotation and also effects due to nondipolar field components. Branson, and also Conway and Stannard [1972], found evidence for a "hot spot" at a System III (1965) longitude of about 200°. De Pater and Dames [1979] confirmed the existence of the hot spot in 1973, but found it to be located at a longitude about 60° higher than reported by Branson. Ground observations have revealed a striking enhancement of UV radiation from sulfur ions in the inner part of the Io torus (see Chap. 6) at about the same longitude as the radio hot spot. Dessler [1980a] has suggested that the two effects are related.

De Pater, using the Westerbork aperture synthesis array, has extensively mapped the synchrotron source region at 1412 MHz [de Pater, 1980a,b] and 4885 MHz

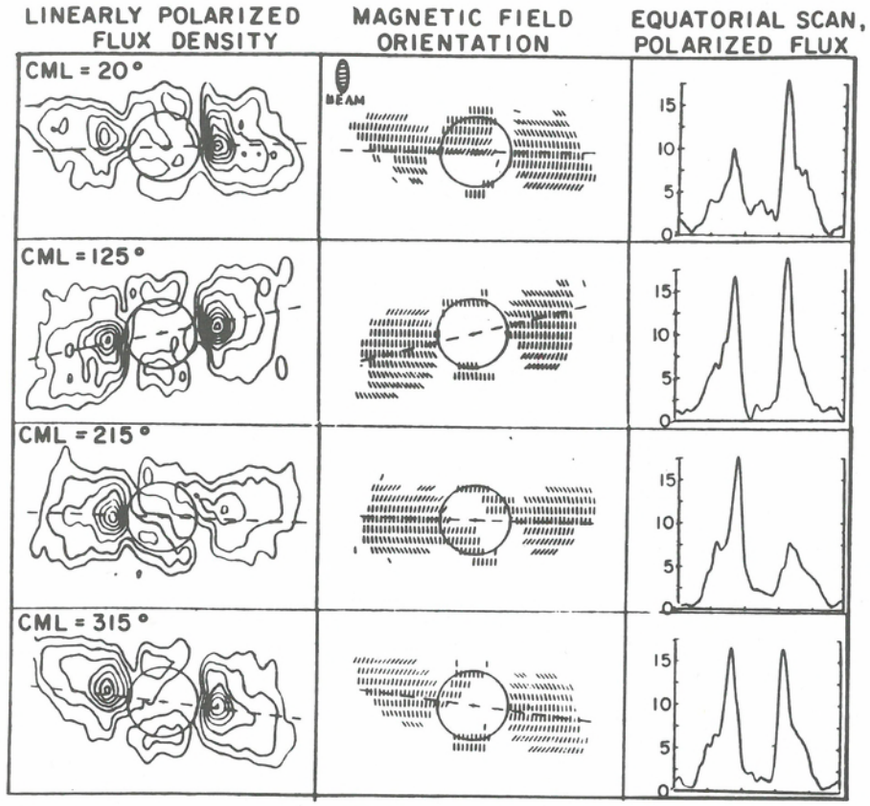

Fig. 7.9. Maps of the linearly polarized flux density at 6 cm wavelength (left-hand panels), magnetic field orientation (center panels) and polarized flux density scans (in Jy) across the magnetic equator. The value of the CML is given in the upper left-hand corner of the first panel for each of the four rows of maps. The projected average magnetic field directions are drawn perpendicular to the measured orientation of the linearly polarized component of the radio emission. Adapted from de Pater [1981].

[de Pater, 1981c]. At 4885 MHz, she constructed for each 15° strip of CML a brightness distribution map of the linearly polarized component, a map of the projected average magnetic field directions (as deduced from the linear polarization direction) and a cross-scan plot of the linearly polarized brightness along the magnetic equator. Examples selected from this series of 24 sets of maps are shown in Figure 7.9.

Assuming the simple dipole model, one would expect the maxima of the total intensity and those of the linearly polarized component to occur at the λ_{III} values of 110° and 290°, and the circularly polarized maxima (of opposite senses) to be at 20° and 200°. As we have seen from Figure 7.6, this is approximately the case. However, it is apparent from de Pater's complete series of maps, that this is far from true in the vicinity of the magnetic equator. Conspicuous anomalies are present in the distribution of both the linear and circularly polarized components. For example, in Figure 7.9, at $\lambda_{III} = 20°$ the brightness center to the right of the planetary disc is much stronger than the one to the left for the linearly polarized intensity. The reverse is true at $\lambda_{III} = 215°$, about 180° of rotation later. Such effects are manifestations of the multipolar magnetic field structure and are related to the hot spot of Branson [1968] and the warped equator of Gerard [1976]. Another curiosity is the previously undetected

emission regions can be seen near the poles at the top and bottom of the planetary disk in Figure 7.9. They are perhaps due to mirroring electrons relatively close to the poles whose orbits are viewed nearly edge-on (i.e., with the line of sight nearly perpendicular to **B**), according to de Pater.

Insofar as Jupiter's magnetosphere is concerned (and hence this book), the ultimate goal of studies of the synchrotron radiation is the creation of the best possible source model incorporating detailed information on the spatial, energy, and pitch-angle distributions of the radiating energetic electrons and how and why these distributions vary with time. The high-resolution measurements of de Pater have made possible the construction of such a model in considerable detail. This model is described in two papers by de Pater [1981a,b] and in her thesis [de Pater, 1980b]. It is undoubtedly the most advanced treatment of the inner magnetosphere that has yet been published and may not be surpassed until measurements made at still higher resolution with the Very Large Array (VLA) in New Mexico are incorporated into a new model.

De Pater's model is discussed in Chapter 5.

7.3. The decameter and hectometer wavelength emission

In the remainder of this chapter we shall be concerned with the complex phenomenology of Jupiter's radio bursts, which are confined to the frequency range below 40 MHz. Despite the fact that the decametric bursts were discovered before the decimetric radiation, the emission mechanism is still only partially understood. On the basis of the large power flux density observed (Fig. 7.1), it is clear that whatever the mechanism (mechanisms) may be, collective interactions between the emitting electrons play a most important role. This is not the case with the synchrotron-emitting electrons. Decametric emission is believed to be near the fundamental of the cyclotron frequency, rather than at its high harmonics as in the case of the synchrotron radiation. The 40 MHz high-frequency cut-off is thus believed to be approximately the electron cyclotron frequency in the region of strongest magnetic field encountered by the emitting electrons. Since there is no evidence of second harmonic emission, the energies of the electrons must be very low in comparison with the synchrotron emitters. These energies are generally believed to be in the tens of keV range.

Another important difference between the two types of emission is in the effect of the surrounding medium. Although the propagation and polarization of the synchrotron radiation are only slightly affected by the plasma adjacent to the emission site, this is not true of the burst radiation. If the emission is in the extraordinary mode, as is generally believed, then it is necessary to assume that the emitted radiation is slightly above the cut-off frequency in order for it to escape the stop zone (see Chap. 9). During escape, its propagation path and polarization may be strongly affected by the plasma and fields it encounters.

The lack of a comprehensive theory to date accounting for the observed radiation phenomenology below 40 MHz can be attributed to several factors. From an observational perspective these include the complex observed phenomenology, and the difficulty of untangling first order from second order effects and of separating out propagation effects and artifacts of observation. All of these have contributed in one form or another to prevent us from answering the fundamental question of locating the radio source. From the point of view of the theorist, the principal obstacles have been the relatively large number of possible plasma instabilities involving various types of interactions in which emitting electrons might participate, the inherent difficulty in formulating mathematical descriptions of these processes and in choosing the important ones, and inadequate knowledge of the characteristics of the magnetospheric

medium. Chapters 9 and 12 are concerned with some of these problems. In the remainder of this chapter we present the extremely diverse phenomenology of the burst radiation, one of our foremost aims being to make it more accessible to those searching for observational constraints with which to limit the theoretical possibilities.

Historical background: from initial discovery to Voyager encounter

We begin this section with a general pre-Voyager overview of some of the major properties of the Jovian emission, specifically of those radio components now commonly referred to as DAM and HOM (for decameter- and hectometer-wavelength emissions, respectively), or collectively as just DAM. (Detailed reviews of the pre-Voyager descriptions may be found in Warwick [1967], Carr and Gulkis [1969], Warwick [1970], Carr and Desch [1976].) Initial observations showed that in addition to being very intense the emission is also elliptically polarized, sometimes in the left-hand sense but more commonly right-hand. The radiation was also observed to be quite sporadic, exhibiting large intensity fluctuations on seconds to tens-of-seconds timescales. This is in sharp contrast to the smoothly and only slightly varying decimeter-wavelength emission (DIM) discussed previously. In addition, observers noted that DAM was invariably confined to frequencies below 40 MHz. The low-frequency emission cut-off, if indeed there was one to be found, was not directly observable owing to the opacity of the Earth's ionosphere at long wavelengths. Ground-based observers were able to establish the existence of DAM at frequencies as low at 4 MHz [Carr et al., 1964; Ellis, 1965; Zabriskie, 1970]. Subsequent earth- and lunar-orbiting satellite observations in the late 1960s and early 1970s [Desch and Carr, 1974; Brown, L. W., 1974; Kaiser, 1977; Desch and Carr, 1978]

1. confirmed the existence of sporadic Jovian emission at frequencies as low as 450 kHz,
2. revealed the broad spectral peak centered at about 8 MHz, and
3. showed that some Io influence over the emission extended down as far as 2 MHz.

Using ground-based telescopes of low spatial, time, and frequency resolution, astronomers recognized that Jupiter possesses a "permanent" DAM dynamic spectrum, that is, landmark emission patterns in the frequency-time domain that reappear when specific central meridian longitudes and Io orbital phases recur. Later, new hierarchies of dynamic spectral pattern organization were found to exist when higher time and frequency resolutions became available. For example, the Io-controlled emission exhibited highly structured and rapidly drifting bursts, called *S* bursts or millisecond bursts, in which there is structure on timescales down to about a millisecond. Continuous monitoring of DAM by fixed-frequency and swept-frequency receivers at a number of observatories

1. revealed the characteristic Jovian-longitude emission zones known as sources A, B, C, and D, and their respective dependence on Io phase,
2. yielded precise measurements of Jupiter's magnetic rotation period, and
3. demonstrated the existence of 11.9-yr periodicities in emission phenomena attributable to changes in the Jovicentric declination of Earth (D_E).

The stability of the source occurrence probability distributions and of dynamic spectral landmarks within sources, the approximate symmetry of sources A and B relative to the tilted magnetic dipole, and the correlations with respect to D_E were generally accepted as due to the geometrical effects of relatively narrow emission beams. These

same synoptic monitoring programs also provided the long data spans necessary to search, with marginal success, for correlations with solar activity, and with no success for effects due to satellites other than Io (e.g., Kaiser and Alexander [1973]).

In short, by the late 1960s the following picture (oversimplified here) was developed from these and other observations and certain assumptions. It was concluded that Jupiter must have several strongly beamed radio sources in both northern and southern hemispheres emitting mostly in the extraordinary mode at or near the local electron cyclotron frequency. Jupiter's global magnetic field must strongly influence the emission properties. This field must have a peak intensity of about 14 G in the northern hemisphere. The field lines must be directed from the vicinity of Jupiter's northern geographic pole toward the southern geographic pole; that is, Jupiter's magnetic field must be flipped relative to Earth's. In fact, these points concerning the field intensity and topology were later confirmed by Pioneer 10 and 11 observations [Smith et al., 1975; Acuña and Ness, 1976c]. Further, in the case of that part of the emission directly stimulated by Io, it was necessary to assume that communication by means of particles or waves occurs between Io and the distant place at which emission occurs. Other radio components independent of Io orbital phase suggested one or more additional controlling influences unrelated to Io.

The Voyager spacecraft observations have been invaluable in complementing and extending the earlier ground-based and satellite efforts in a number of ways. (An overview of the Voyager Planetary Radio Astronomy results can be found in Boischot et al. [1981].) Briefly, because the Voyager observations were free of ionospheric scintillation effects and were of sufficient sensitivity and frequency resolution, another level of structure became apparent in the frequency-time dynamic spectra. For example, the frequency-time landmark features were resolved into many nested spectral arcs, which appeared like rows of opening and closing parentheses of smoothly varying size and curvature. Two distinct classes of arcs became apparent: *greater arcs* and *lesser arcs*, generally distinguishable by their frequency extent and curvatures. Greater arcs can extend from ~1 MHz up to 39.5 MHz; the lesser arcs are more limited in frequency extent, rarely exceeding 15 MHz peak frequency. In addition, Voyager was able to provide the first information on the behavior of the emissions as observed from above Jupiter's nightside hemisphere.

General properties

Spectral characteristics. As has been mentioned, early ground-based and satellite studies had established a high frequency cut-off at about 40 MHz and a broad peak centered at about 8-MHz in the time-averaged flux spectrum. The Voyager observations confirmed these features, and by virtue of greatly increased sensitivity and frequency resolution, made possible an accurate determination of the entire spectrum of the burst emission from 40 MHz down to the lowest frequencies at which radio propagation is possible. This spectrum together with that of the synchrotron component constitute Jupiter's nonthermal emission; the spectra are shown in Figure 7.1. In this figure the peak in the DAM range is broad, extending over a band about 4 MHz wide centered on about 10 MHz. The high-frequency shoulder is much steeper than that at low frequencies and corresponds to a spectral index (i.e., the exponent n in $S \propto f^n$) of about -6. The Voyager results confirmed that there is indeed a high-frequency cut-off at 39.5 MHz, and that it is of natural origin, not simply an artifact due to inadequate sampling of weak events. This spectral boundary, labeled "magnetic cut-off" in Figure 7.1, has long been suspected to represent the maximum electron cyclotron frequency occurring in the region of emission, an idea that is strongly supported by the Pioneer and Voyager magnetometer results. The drop-off below about 2 MHz, on the other hand, may be due in part to propagation effects induced by the dense Io plasma torus.

The Voyager observations have extended the range to lower frequencies so that a minor peak is apparent at about 100 kHz. This peak has an intensity level 1.5 orders of magnitude below the principal peak, and the shoulder on the low-frequency side extends to the boundary for freely propagating electromagnetic radiation, labeled "plasma cut-off" in Figure 7.1. This cut-off varies with both the propagation path and with time; it is essentially the maximum plasma frequency between source and observer and is believed to occur in the 1 to 10 kHz range. Below the plasma cutoff lies the realm of the plasma waves – waves that are bound to the medium. They are the subject of Chapter 8.

Examination of frequency-time dynamic spectra, discussed in detail below, shows that several distinct types of emission make up the spectrum shown in Figure 7.1. The "greater arcs" can extend from at least 1 MHz up to the 39.5-MHz cut-off, whereas the "lesser arcs" are more limited in frequency extent. It is these two components that collectively make up the single flux peak near 10 MHz. The low-frequency secondary hump is also made up of two separate sources, the narrow band (n) and broadband (b) kilometric (KOM) radiation, discussed later.

By integrating the power flux density curve over the entire frequency range and assuming that the radiation is emitted uniformly and isotropically over $4\pi sr$, we can arrive at a crude estimate of the total (average) radiated power. The value obtained is 3×10^{11} W, a number that is very likely an overestimate since the DAM component, at least, is not emitted isotropically. A lower-limit estimate of the average value of the total radiated power is probably 6×10^9 W, arrived at by assuming an emission cone conical-sheet thickness of 5°.

Temporal structure and dynamic spectrum. Frequency-time dynamic spectra of Jovian emission are extremely complex, although well ordered and even predictable. Figure 7.10 shows a 10-h spectrum from Voyager observations in which increasing darkness is proportional to increasing radio intensity. The spectrum covers the frequency range from 20 kHz to 40 MHz. The emission is organized into several hierarchies according to timescale. Most apparent is the organization into individual *storms*; for example, the event from 03 hr to 05 hr SCET (spacecraft event time) centered at 20 MHz is a single storm. Later we shall see that because this storm is associated with a particular longitude region and Io's orbital phase was not within two special zones, it is referred to as a non-Io-A storm (see Table 7.4). These active periods are quite episodic. Storms in some frequency ranges may last up to several hours with long periods of complete radio quiet separating them. It is on this timescale that the permanent Jovian dynamic spectrum appears.

Detailed structure is also apparent within each storm in these relatively low-resolution spectra and here a second hierarchy appears. On a timescale of minutes, we observe the ubiquitous *spectral arcs*, one of the principal Voyager radio astronomy discoveries. Note the well-defined closing parenthesis-shaped arcs which make up the non-Io-A storm just described. In contrast, at 22 hr to 00 hr a non-Io-B storm occurred in which the arcs are oriented in opening-parenthesis fashion. This is another example of the remarkable repeatability of the Jovian radio morphology: the arcs are always oriented in the same way within a given storm class so that they constitute another level of permanent dynamic spectra. The detailed morphology of these landmark features is described later.

Modulations appear on a timescale of seconds, some of which are intrinsic to the source itself, and some of which are not. An example is shown in Figure 7.11 which has

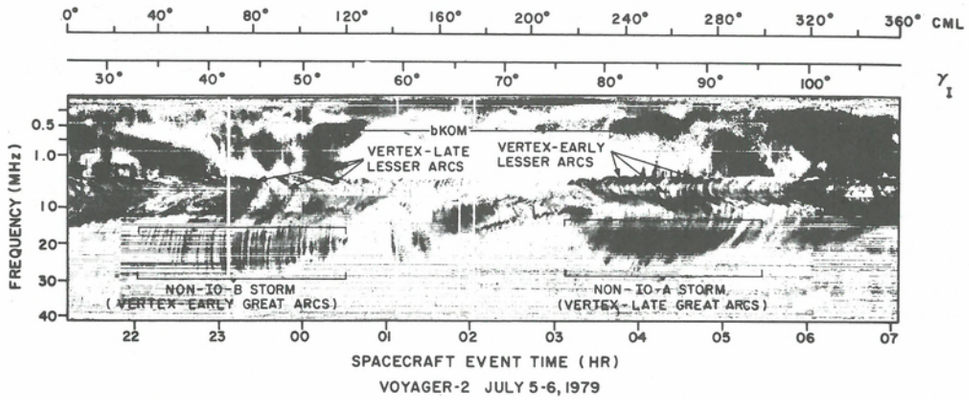

Fig. 7.10. A representative dynamic spectrum of Jupiter's low frequency radio emissions during one complete rotation of the planet. The darkness of the grey shading is proportional to signal intensity, plotted here as a function of frequency and time. The frequency axis is actually divided into two distinct bands that adjoin at about 1.3 MHz; the low frequency band consists of 70 frequency channels spaced at 19 kHz intervals between 1 and 1326 kHz, and the high frequency band is composed of 128 channels spaced 307 kHz apart between 1.2 and 40.5 MHz. At frequencies above 20 MHz, two major DAM "great arc" storms can be seen centered on about 23 hr and 04 hr spacecraft event time. At frequencies between a few MHz and about 15 MHz the "lesser arc" DAM can be seen with "vertex-late" curvature after 03 hr. Some of the DAM arcs appear to extend to below 0.5 MHz in the low frequency band where the frequency scale is greatly expanded.

been adapted from work by Riihimaa [1971]. This figure is again in the format of a dynamic spectrum, but at much higher frequency and time resolution than those shown previously. The negatively drifting (i.e., $df/dt < 0$) emission features are called *modulation lanes*. Generally, modulation lanes can have drift rates of from -150 to $+150$ kHz/s; those shown in the figure drift at about -150 kHz/s. By way of contrast, the greater arcs in this frequency range drift about an order of magnitude slower on the average. Vertical gaps, centered at about 16 and 20 s, break up the envelopes of the modulation lanes. Intensity structure on this 1 to 5 s timescale, as illustrated by these envelopes and gaps in Figure 7.11, are commonplace in groundbased data and are referred to as *L* (long) *bursts*. Douglas and Smith [1967] first demonstrated that these temporal signatures are due primarily to the infuence of interplanetary scintillation. This modulation is most apparent in data taken at significant distances from Jupiter. *L*-burst groups also experience a 30–60 s modulation caused by the Earth's ionosphere. Thus we might expect, and indeed there is some evidence, that close to Jupiter most but not all of the radiation is in the form of relatively long bursts of emission. These long bursts are subsequently broken up into *L*-burst trains by scintillation during propagation to Earth. The implication here is that the fundamental timescale of the original burst from which the *L* bursts is formed is actually tens of seconds or minutes and may simply correspond to the 3- and 6-min timescale of the arc structure [Genova and Leblanc, 1981]. The observed modulation-lane structure must be primarily intrinsic to the source, or at least to propagation effects in the immediate neighborhood of the source, because the drift rates are principally dependent on Jovian longitude [Riihimaa, 1974]. However, a secondary dependence on the solar elongation at the time of the observation has been reported [Riihimaa, 1979]. These conclusions have of necessity been drawn from Earth-based observations because the Voyager radio astronomy instrument is incapable of resolving modulation-lane structure.

Table 7.4. *Components of Jupiter's decametric emissions*

Source designation	CML range[a]	γ_{Io} range[a]	Maximum frequency (MHz)	Dominant polarization	Arc curvature (vertex)	Notes
Io-D	0°–200°	95°–130°	18	LH	Early	Also called "fourth source"
Io-B	15°–240° (105°–185°)	40°–110° (80°–110°)	39.5	RH	Early	Also called "early source"
non-Io-B	80°–200°	0°–360°	38	RH	Early	Weak from above day hemisphere but strong when viewed from above night hemisphere
Io-A	180°–300° (200°–270°)	180°–260° (205°–260°)	38	RH	Late	Also called "main source"
non-Io-A	200°–300° (230°–280°)	0°–360°	38	RH	Late	Strong from above day hemisphere but weak when viewed from above night hemisphere
Io-C	280°–60° (300°–20°)	200°–260° (225°–260°)	36	RH and LH	Late	Also called "third source"
non-Io-C	300°–360°	0°–360°	32	RH and LH	Late	Moderately strong from above day hemisphere and very weak when viewed from above night side

[a] Numbers in parentheses give widths at half-maximum for the major sources as observed from Earth at frequencies near 20 MHz.